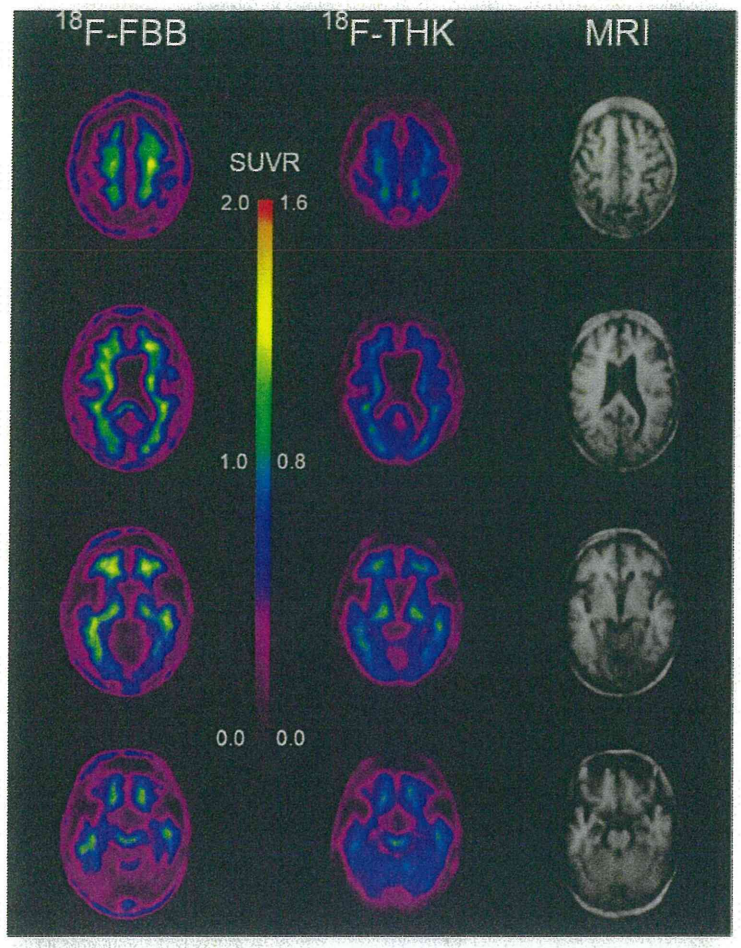

Figure 4 ^{18}F-THK523 and ^{118}F-florbetaben positron emission tomography scans in a progressive supranuclear palsy patient. Representative ^{18}F-florbetaben (^{18}F-FBB, left) and ^{18}F-THK523 (^{18}F-THK, right) transaxial images at three different brain levels of a 79–year-old PSP patient with a Mini Mental State Examination score of 26. Visual inspection reveals no cortical retention of either ^{18}F-THK523 or ^{18}F-florbetaben, despite a postmortem immunohistological examination (see Figure 3 5 months after PET evaluation), confirming the presence of tau lesions. SUVR, Standardised uptake value ratio.

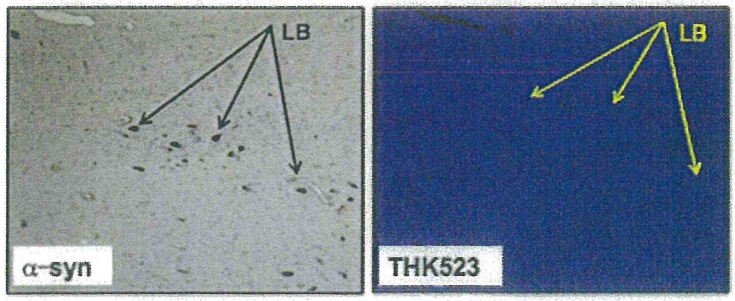

Figure 5 THK523 does not bind to Lewy bodies in Parkinson's disease patient. Microscopy of 5-μm serial sections from the substantia nigra of a Parkinson's disease patient. The left image (α-syn shows the first of two serial sections. It immunostained with an α-synuclein antibody to detect Lewy bodies (LB) in the substantia nigra. The black arrows indicate the positioning of LBs. The same region of tissue was subsequently imaged for the adjacent sections, which were treated with THK523. The positions indicated by the black arrows in the left panel were transferred to the adjacent THK523 serial section and are indicated by the yellow arrows (THK523). The absence of fluorescence staining indicates that THK523 does not bind to α-synuclein containing Lewy bodies in the same tissue region. Tissue sections were imaged using a Zeiss microscope and an AxioCam digital camera at 5× original magnification.

binding to NFTs, our fluorescence studies obtained at high tracer concentrations—10,000-fold higher than the concentrations typically achieved during a PET scan—demonstrated inconsistent THK523 staining of Aβ plaques. THK523 stained the dense core of some Aβ plaques in the frontal cortex of AD sections but did not stain dense Aβ plaques in the hippocampus (Figure 1, right panel). It is noteworthy that variable staining of NFTs at high concentrations of PiB has also been reported [52]. In addition to previous reports of *in vitro* studies [29,30], several lines of evidence support the notion that THK523 selectively binds to PHF-tau and does not bind to Aβ *in vivo*: (1) Cortical THK523 retention is significantly higher in AD; (2) THK523 retention follows the known distribution of PHF-tau in the AD brain; (3) PiB and THK523 show different brain regional distribution patterns; (4) hippocampal THK523 retention significantly correlated with cognitive parameters, but hippocampal PiB retention did not; and (5) hippocampal THK523 retention significantly correlated with hippocampal volume, but hippocampal PiB retention did not [32].

The selectivity of THK523 for tau over other β-sheet aggregated proteins was further demonstrated by fluorescence microscopy studies showing the absence of THK523 fluorescence in brain sections exhibiting immunolabelled α-synuclein-containing Lewy bodies (Figure 5, right panel).

The PSP patient showed neither ^{18}F-THK523 nor ^{18}F-florbetaben retention in the brain, suggesting the absence not only of Aβ plaques but also of tau deposits. Neuropathological examination of the brain confirmed the absence of Aβ plaques; however, typical tau lesions were present in different brain regions that were not stained by THK523. Given the ultrastructural diversity of tau aggregates, the information derived from these THK523 studies is highly valuable for the future design of tau imaging ligands.

Conclusion

In the present study, we have demonstrated that THK523 selectively binds to PHF-tau with negligible binding to PSP, CBD and PiD tau aggregates, as well as to Aβ and α-synuclein aggregates. The results of this study also show that novel tracers that bind to non-PHF tau aggregates are needed.

Abbreviations

AD: Alzheimer's disease; Aβ: Amyloid-β; CBD: Corticobasal degeneration; CDR: Clinical Dementia Rating Scale; CDR-SOB: Clinical Dementia Rating Scale–Sum of Boxes; CSF: Cerebrospinal fluid; FTLD: Frontotemporal lobar degeneration; GM: Grey matter; MMSE: Mini Mental State Examination; NFT: Neurofibrillary tangle; PET: Positron emission tomography; PiB: Pittsburgh compound B; PiD: Pick's disease; PSP: Progressive supranuclear palsy; ROI: Region of interest; SF: Straight filament; SUV: Standardised uptake value; TF: Twisted filament.

Competing interests

The authors declare that they have no competing interests.

Authors' contributions

VLV, MTF-T, KY, NO and CLM designed the experiments. SF, RSM, RH, KY, YK and NO designed and manufactured THK523. LT and IB planned and conducted the human brain section immunostaining experiments. CAM planned and conducted the pathological characterisation of human brain samples. VL and CCR planned and coordinated human PET studies. MTF-T and VLV drafted the manuscript. All authors read and approved the final manuscript.

Acknowledgements

We thank Fairlie Hinton and Geoff Pavey from the Victorian Brain Bank Network (VBBN) for sourcing and preparing the human brain tissue (HREC University of Melbourne 9414748). The VBBN is supported by The Florey Institute of Neuroscience and Mental Health, The Alfred and the Victorian Forensic Institute of Medicine, and it is funded by Australia's National Health & Medical Research Council (NHMRC) and Parkinson's Victoria. The research was supported in part by Alzheimer's Drug Discovery Foundation Research Grant 20101208 AFTD and NHMRC project grant 1044361.

Author details

[1]The Florey Institute of Neuroscience and Mental Health, 30 Royal Parade, Parkville, 3052 Melbourne, Victoria, Australia. [2]Department of Nuclear Medicine & Centre for PET, Austin Health, 145 Studley Road, Heidelberg, 3084 Melbourne, Victoria, Australia. [3]Department Pharmacology, Tohoku University School of Medicine, Sendai, Japan. [4]Department of Anatomical Pathology, The Alfred Hospital, Monash University, Melbourne, Australia. [5]Innovation of New Biomedical Engineering Center, Tohoku University, Sendai, Japan.

Received: 11 July 2013 Accepted: 13 February 2014
Published: 26 February 2014

References

1. Masters CL, Cappai R, Barnham KJ, Villemagne VL: **Molecular mechanisms for Alzheimer's disease: implications for neuroimaging and therapeutics.** *J Neurochem* 2006, **97**:1700–1725.
2. van der Zee J, Sleegers K, Van Broeckhoven C: **Invited article: the Alzheimer disease–frontotemporal lobar degeneration spectrum.** *Neurology* 2008, **71**:1191–1197.
3. Braak H, Braak E: **Morphological criteria for the recognition of Alzheimer's disease and the distribution pattern of cortical changes related to this disorder.** *Neurobiol Aging* 1994, **15**:355–356. discussion 379–380.
4. Corder EH, Woodbury MA, Volkmann I, Madsen DK, Bogdanovic N, Winblad B: **Density profiles of Alzheimer disease regional brain pathology for the Huddinge Brain Bank: pattern recognition emulates and expands upon Braak staging.** *Exp Gerontol* 2000, **35**:851–864.
5. The National Institute on Aging and Reagan Institute Working Group on Diagnostic Criteria for the Neuropathological Assessment of Alzheimer's Disease: **Consensus recommendations for the postmortem diagnosis of Alzheimer's disease.** *Neurobiol Aging* 1997, **18**:S1–S2.
6. Delacourte A: **Tauopathies: recent insights into old diseases.** *Folia Neuropathol* 2005, **43**:244–257.
7. King ME, Ghoshal N, Wall JS, Binder LI, Ksiezak-Reding H: **Structural analysis of Pick's disease-derived and *in vitro*-assembled tau filaments.** *Am J Pathol* 2001, **158**:1481–1490.
8. Scaravilli T, Tolosa E, Ferrer I: **Progressive supranuclear palsy and corticobasal degeneration: lumping versus splitting.** *Mov Disord* 2005, **20**:S21–S28.
9. Uchihara T, Tsuchiya K: **Neuropathology of Pick body disease.** *Handb Clin Neurol* 2008, **89**:415–430.
10. Mohorko N, Bresjanac M: **[Tau protein and human tauopathies: an overview] [in Slovenian].** *Zdrav Vestn* 2008, **77**:II-35–II-41.
11. Delacourte A, Buée L: **Tau pathology: a marker of neurodegenerative disorders.** *Curr Opin Neurol* 2000, **13**:371–376.
12. Villemagne VL, Furumoto S, Fodero-Tavoletti M, Harada R, Mulligan RS, Kudo Y, Masters CL, Yanai K, Rowe CC, Okamura N: **The challenges of tau imaging.** *Future Neurol* 2012, **7**:409–421.
13. Dickson DW: **Neuropathology of Pick's disease.** *Neurology* 2001, **56**:S16–S20.

14. Josephs KA, Whitwell JL, Dickson DW, Boeve BF, Knopman DS, Petersen RC, Parisi JE, Jack CR Jr: **Voxel-based morphometry in autopsy proven PSP and CBD.** *Neurobiol Aging* 2008, **29**:280–289.
15. Dickson DW: **Neuropathologic differentiation of progressive supranuclear palsy and corticobasal degeneration.** *J Neurol* 1999, **246**:II6–II15.
16. Cairns NJ, Bigio EH, Mackenzie IRA, Neumann M, Lee VM, Hatanpaa KJ, White CL 3rd, Schneider JA, Grinberg LT, Halliday G, Duyckaerts C, Lowe JS, Holm IE, Tolnay M, Okamoto K, Yokoo H, Murayama S, Woulfe J, Munoz DG, Dickson DW, Ince PG, Trojanowski JQ, Mann DM, Consortium for Frontotemporal Lobar Degeneration: **Neuropathologic diagnostic and nosologic criteria for frontotemporal lobar degeneration: consensus of the Consortium for Frontotemporal Lobar Degeneration.** *Acta Neuropathol* 2007, **114**:5–22.
17. Boxer AL, Geschwind MD, Belfor N, Gorno-Tempini ML, Schauer GF, Miller BL, Weiner MW, Rosen HJ: **Patterns of brain atrophy that differentiate corticobasal degeneration syndrome from progressive supranuclear palsy.** *Arch Neurol* 2006, **63**:81–86.
18. Jack CR Jr, Knopman DS, Jagust WJ, Shaw LM, Aisen PS, Weiner MW, Petersen RC, Trojanowski JQ: **Hypothetical model of dynamic biomarkers of the Alzheimer's pathological cascade.** *Lancet Neurol* 2010, **9**:119–128.
19. Gozes I, Stewart A, Morimoto B, Fox A, Sutherland K, Schmeche D: **Addressing Alzheimer's disease tangles: from NAP to AL-108.** *Curr Alzheimer Res* 2009, **6**:455–460.
20. Hampel H, Blennow K, Shaw LM, Hoessler YC, Zetterberg H, Trojanowski JQ: **Total and phosphorylated tau protein as biological markers of Alzheimer's disease.** *Exp Gerontol* 2010, **45**:30–40.
21. Wada T, Miyata T, Sakai H, Kurokawa K: **β2-microglobulin and renal bone disease.** *Perit Dial Int* 1999, **19**:S413–S416.
22. Wider C, Uitti RJ, Wszolek ZK, Fang JY, Josephs KA, Baker MC, Rademakers R, Hutton ML, Dickson DW: **Progranulin gene mutation with an unusual clinical and neuropathologic presentation.** *Mov Disord* 2008, **23**:1168–1173.
23. Wischik C, Staff R: **Challenges in the conduct of disease-modifying trials in AD: practical experience from a phase 2 trial of Tau-aggregation inhibitor therapy.** *J Nutr Health Aging* 2009, **13**:367–369.
24. Cui M: **Past and recent progress of molecular imaging probes for β-amyloid plaques in the brain.** *Curr Med Chem* 2014, **21**:82–112.
25. Klunk WE, Engler H, Nordberg A, Wang Y, Blomqvist G, Holt DP, Bergström M, Savitcheva I, Huang GF, Estrada S, Ausén B, Debnath ML, Barletta J, Price JC, Sandell J, Lopresti BJ, Wall A, Koivisto P, Antoni G, Mathis CA, Långström B: **Imaging brain amyloid in Alzheimer's disease with Pittsburgh Compound-B.** *Ann Neurol* 2004, **55**:306–319.
26. Rowe CC, Ng S, Ackermann U, Gong SJ, Pike K, Savage G, Cowie TF, Dickinson KL, Maruff P, Darby D, Smith C, Woodward M, Merory J, Tochon-Danguy H, O'Keefe G, Klunk WE, Mathis CA, Price JC, Masters CL, Villemagne VL: **Imaging β-amyloid burden in aging and dementia.** *Neurology* 2007, **68**:1718–1725.
27. Clark CM, Schneider JA, Bedell BJ, Beach TG, Bilker WB, Mintun MA, Pontecorvo MJ, Hefti F, Carpenter AP, Flitter ML, Krautkramer MJ, Kung HF, Coleman RE, Doraiswamy PM, Fleisher AS, Sabbagh MN, Sadowsky CH, Reiman EP, Zehntner SP, Skovronsky DM, AV45-A07 Study Group: **Use of florbetapir-PET for imaging β-amyloid pathology.** *JAMA* 2011, **305**:275–283.
28. Vandenberghe R, Van Laere K, Ivanoiu A, Salmon E, Bastin C, Triau E, Hasselbalch S, Law I, Andersen A, Korner A, Minthon L, Garraux G, Nelissen N, Bormans G, Buckley C, Owenius R, Thurfjell L, Farrar G, Brooks DJ: **^{18}F-flutemetamol amyloid imaging in Alzheimer disease and mild cognitive impairment: a phase 2 trial.** *Ann Neurol* 2010, **68**:319–329.
29. Fodero-Tavoletti MT, Okamura N, Furumoto S, Mulligan RS, Connor AR, McLean CA, Cao D, Rigopoulos A, Cartwright GA, O'Keefe G, Gong S, Adlard PA, Barnham KJ, Rowe CC, Masters CL, Kudo Y, Cappai R, Yanai K, Villemagne VL: **^{18}F-THK523: a novel *in vivo* tau imaging ligand for Alzheimer's disease.** *Brain* 2011, **134**:1089–1100.
30. Harada R, Okamura N, Furumoto S, Tago T, Maruyama M, Higuchi M, Yoshikawa T, Arai H, Iwata R, Kudo Y, Yanai K: **Comparison of the binding characteristics of [^{18}F]THK-523 and other amyloid imaging tracers to Alzheimer's disease pathology.** *Eur J Nucl Med Mol Imaging* 2013, **40**:125–132.
31. Okamura N, Suemoto T, Furumoto S, Suzuki M, Shimadzu H, Akatsu H, Yamamoto T, Fujiwara H, Nemoto M, Maruyama M, Arai H, Yanai K, Sawada T, Kudo Y: **Quinoline and benzimidazole derivatives: candidate probes for *in vivo* imaging of tau pathology in Alzheimer's disease.** *J Neurosci* 2005, **25**:10857–10862.
32. Villemagne VL, Furumoto S, Fodero-Tavoletti MT, Mulligan RS, Hodges J, Harada R, Yates P, Piguet O, Pejoska S, Doré V, Yanai K, Masters CL, Kudo Y, Rowe CC, Okamura N: ***In vivo* evaluation of a novel tau imaging tracer for Alzheimer's disease.** *Eur J Nucl Med Mol Imaging* 2014. [Epub ahead of print]. doi:10.1007/s00259-013-2681-7.
33. Hauw JJ, Daniel SE, Dickson D, Horoupian DS, Jellinger K, Lantos PL, McKee A, Tabaton M, Litvan I: **Preliminary NINDS neuropathologic criteria for Steele-Richardson-Olszewski syndrome (progressive supranuclear palsy).** *Neurology* 1994, **44**:2015–2019.
34. Lowe J: **Part 7: Frontotemporal Lobar Degeneration and Amyotrophic Lateral Sclerosis/Motor Neuron Disease. Chapter 40: Introduction.** In *Neurodegeneration: The Molecular Pathology of Dementia and Movement Disorders.* 2nd edition. Edited by Dickson D, Weller RO. Oxford, UK: Wiley-Blackwell; 2011:389–390.
35. Culvenor JG, McLean CA, Cutt S, Campbell BC, Maher F, Jäkälä P, Hartmann T, Beyreuther K, Masters CL, Li QX: **Non-Aβ component of Alzheimer's disease amyloid (NAC) revisited: NAC and α-synuclein are not associated with Aβ amyloid.** *Am J Pathol* 1999, **155**:1173–1181.
36. Culvenor JG, Henry A, Hartmann T, Evin G, Galatis D, Friedhuber A, Jayasena UL, Underwood JR, Beyreuther K, Masters CL, Cappai R: **Subcellular localization of the Alzheimer's disease amyloid precursor protein and derived polypeptides expressed in a recombinant yeast system.** *Amyloid* 1998, **5**:79–89.
37. Villemagne V, Fodero-Tavoletti M, Furumoto S, Mulligan RS, Hodges J, Piguet O, Pejoska S, Kudo Y, Masters C, Yanai K, Rowe C, Okamura N: ***In vivo* tau imaging in Alzheimer's disease and other dementias.** *Alzheimers Dement* 2012, **8**:699.
38. Villemagne VL, Fodero-Tavoletti MT, Pike KE, Cappai R, Masters CL, Rowe CC: **The ART of loss: Aβ imaging in the evaluation of Alzheimer's disease and other dementias.** *Mol Neurobiol* 2008, **38**:1–15.
39. Rowe CC, Ackerman U, Browne W, Mulligan R, Pike KL, O'Keefe G, Tochon-Danguy H, Chan G, Berlangieri SU, Jones G, Dickinson-Rowe KL, Kung HP, Zhang W, Kung MP, Skovronsky D, Dyrks T, Holl G, Krause S, Friebe M, Lehman L, Lindemann S, Dinkelborg LM, Masters CL, Villemagne VL: **Imaging of amyloid β in Alzheimer's disease with ^{18}F-BAY94-9172, a novel PET tracer: proof of mechanism.** *Lancet Neurol* 2008, **7**:129–135.
40. Villemagne VL, Pike KE, Chételat G, Ellis KA, Mulligan RS, Bourgeat P, Ackermann U, Jones G, Szoeke C, Salvado O, Martins R, O'Keefe G, Mathis CA, Klunk WE, Ames D, Masters CL, Rowe CC: **Longitudinal assessment of Aβ and cognition in aging and Alzheimer disease.** *Ann Neurol* 2011, **69**:181–192.
41. Good CD, Johnsrude IS, Ashburner J, Henson RN, Friston KJ, Frackowiak RS: **A voxel-based morphometric study of ageing in 465 normal adult human brains.** *Neuroimage* 2001, **14**:21–36.
42. Sergeant N, Bretteville A, Hamdane M, Caillet-Boudin ML, Grognet P, Bombois S, Blum D, Delacourte A, Pasquier F, Vanmechelen E, Schraen-Maschke S, Buée L: **Biochemistry of Tau in Alzheimer's disease and related neurological disorders.** *Expert Rev Proteomics* 2008, **5**:207–224.
43. Williams DR, Holton JL, Strand C, Pittman A, de Silva R, Lees AJ, Revesz T: **Pathological tau burden and distribution distinguishes progressive supranuclear palsy-parkinsonism from Richardson's syndrome.** *Brain* 2007, **130**:1566–1576.
44. Yamada T, McGeer PL, McGeer EG: **Appearance of paired nucleated, Tau-positive glia in patients with progressive supranuclear palsy brain tissue.** *Neurosci Lett* 1992, **135**:99–102.
45. Dickson DW, Bergeron C, Chin SS, Duyckaerts C, Horoupian D, Ikeda K, Jellinger K, Lantos PL, Lippa CF, Mirra SS, Tabaton M, Vonsattel JP, Wakabayashi K, Litvan I, Office of Rare Diseases of the National Institutes of Health: **Office of Rare Diseases neuropathologic criteria for corticobasal degeneration.** *J Neuropathol Exp Neurol* 2002, **61**:935–946.
46. Buée L, Delacourte A: **Comparative biochemistry of tau in progressive supranuclear palsy, corticobasal degeneration, FTDP-17 and Pick's disease.** *Brain Pathol* 1999, **9**:681–693.
47. Arima K: **Ultrastructural characteristics of tau filaments in tauopathies: immuno-electron microscopic demonstration of tau filaments in tauopathies.** *Neuropathology* 2006, **26**:475–483.
48. Maruyama M, Shimada H, Suhara T, Shinotoh H, Ji B, Maeda J, Zhang MR, Trojanowski JQ, Lee VM, Ono M, Masamoto K, Takano H, Sahara N, Iwata N, Okamura N, Furumoto S, Kudo Y, Chang Q, Saido TC, Takashima A, Lewis J,

Jang MK, Aoki I, Ito H, Higuchi M: **Imaging of tau pathology in a tauopathy mouse model and in Alzheimer patients compared to normal controls.** *Neuron* 2013, **79**:1094–1108.
49. Crowther RA: **Straight and paired helical filaments in Alzheimer disease have a common structural unit.** *Proc Natl Acad Sci U S A* 1991, **88**:2288–2292.
50. Bulic B, Pickhardt M, Mandelkow EM, Mandelkow E: **Tau protein and tau aggregation inhibitors.** *Neuropharmacology* 2010, **59**:276–289.
51. Agdeppa ED, Kepe V, Liu J, Flores-Torres S, Satyamurthy N, Petric A, Cole GM, Small GW, Huang SC, Barrio JR: **Binding characteristics of radiofluorinated 6-dialkylamino-2-naphthylethylidene derivatives as positron emission tomography imaging probes for β-amyloid plaques in Alzheimer's disease.** *J Neurosci* 2001, **21**:RC189.
52. Ikonomovic MD, Klunk WE, Abrahamson EE, Mathis CA, Price JC, Tsopelas ND, Lopresti BJ, Ziolko S, Bi W, Paljug WR, Debnath ML, Hope CE, Isanski BA, Hamilton RL, DeKosky ST: **Post-mortem correlates of *in vivo* PiB-PET amyloid imaging in a typical case of Alzheimer's disease.** *Brain* 2008, **131**:1630–1645.

doi:10.1186/alzrt240
Cite this article as: Fodero-Tavoletti *et al.*: Assessing THK523 selectivity for tau deposits in Alzheimer's disease and non–Alzheimer's disease tauopathies. *Alzheimer's Research & Therapy* 2014 6:11.

doi:10.1093/brain/awu064 Brain 2014: 137; 1762–1771 | 1762

BRAIN
A JOURNAL OF NEUROLOGY

Non-invasive assessment of Alzheimer's disease neurofibrillary pathology using ^{18}F-THK5105 PET

Nobuyuki Okamura,[1] Shozo Furumoto,[2] Michelle T. Fodero-Tavoletti,[3,4] Rachel S. Mulligan,[4] Ryuichi Harada,[1] Paul Yates,[4] Svetlana Pejoska,[4] Yukitsuka Kudo,[5] Colin L. Masters,[3,6] Kazuhiko Yanai,[1,2] Christopher C. Rowe[4] and Victor L. Villemagne[3,4]

1 Department of Pharmacology, Tohoku University School of Medicine, Sendai, Japan
2 Cyclotron and Radioisotope Centre, Tohoku University, Sendai, Japan
3 The Florey Institute of Neuroscience and Mental Health, The University of Melbourne, Australia
4 Centre for PET, Austin Health, Melbourne, Australia
5 Clinical Research, Innovation and Education Centre, Tohoku University Hospital, Sendai, Japan
6 The Mental Health Research Institute, Melbourne, Australia

Correspondence to: Nobuyuki Okamura,
Department of Pharmacology,
Tohoku University School of Medicine,
2-1 Seiryo-machi, Aoba-ku,
Sendai, 9808575, Japan
E-mail: nookamura@med.tohoku.ac.jp

Non-invasive imaging of tau pathology in the living brain would be useful for accurately diagnosing Alzheimer's disease, tracking disease progression, and evaluating the treatment efficacy of disease-specific therapeutics. In this study, we evaluated the clinical usefulness of a novel tau-imaging positron emission tomography tracer ^{18}F-THK5105 in 16 human subjects including eight patients with Alzheimer's disease (three male and five females, 66–82 years) and eight healthy elderly controls (three male and five females, 63–76 years). All participants underwent neuropsychological examination and 3D magnetic resonance imaging, as well as both ^{18}F-THK5105 and ^{11}C-Pittsburgh compound B positron emission tomography scans. Standard uptake value ratios at 90–100 min and 40–70 min post-injection were calculated for ^{18}F-THK5105 and ^{11}C-Pittsburgh compound B, respectively, using the cerebellar cortex as the reference region. As a result, significantly higher ^{18}F-THK5105 retention was observed in the temporal, parietal, posterior cingulate, frontal and mesial temporal cortices of patients with Alzheimer's disease compared with healthy control subjects. In patients with Alzheimer's disease, the inferior temporal cortex, which is an area known to contain high densities of neurofibrillary tangles in the Alzheimer's disease brain, showed prominent ^{18}F-THK5105 retention. Compared with high frequency (100%) of ^{18}F-THK5105 retention in the temporal cortex of patients with Alzheimer's disease, frontal ^{18}F-THK5105 retention was less frequent (37.5%) and was only observed in cases with moderate-to-severe Alzheimer's disease. In contrast, ^{11}C-Pittsburgh compound B retention was highest in the posterior cingulate cortex, followed by the ventrolateral prefrontal, anterior cingulate, and superior temporal cortices, and did not correlate with ^{18}F-THK5105 retention in the neocortex. In healthy control subjects, ^{18}F-THK5105 retention was ~10% higher in the mesial temporal cortex than in the neocortex. Notably, unlike ^{11}C-Pittsburgh compound B, ^{18}F-THK5105 retention was significantly correlated with cognitive parameters, hippocampal and whole brain grey matter volumes, which was consistent with findings from previous post-mortem studies showing significant correlations of neurofibrillary tangle density with dementia severity or neuronal loss. From these results, ^{18}F-THK5105 positron emission tomography is considered to be useful for the non-invasive assessment of tau pathology in the living brain. This technique would be applicable to the longitudinal evaluation of tau deposition and allow a better understanding of the pathophysiology of Alzheimer's disease.

Received December 11, 2013. Revised January 12, 2014. Accepted February 4, 2014. Advance Access publication March 27, 2014

Keywords: Alzheimer's disease; Alzheimer's disease pathology; amyloid; positron emission tomography; PET

Abbreviations: CDR = clinical dementia rating; MMSE = Mini-Mental State Examination; PiB = Pittsburgh compound B; SOB = sum of boxes; SUV = standardized uptake value; SUVR = ratio of regional SUV to cerebellar cortex SUV ratio

Introduction

Senile plaques and neurofibrillary tangles are considered the major pathological hallmarks of Alzheimer's disease (Braak and Braak, 1991). Senile plaques consist of extracellular aggregates of amyloid-β peptide cleaved from a longer amyloid precursor protein (Masters *et al.*, 2006). The neocortical deposition of senile plaques is considered one of the earliest pathological alterations in Alzheimer's disease and is observed even in the presymptomatic stages (Mintun *et al.*, 2006; Rowe *et al.*, 2007; Price *et al.*, 2009). Recently proposed research diagnostic criteria for preclinical Alzheimer's disease include cognitively intact elderly with abnormal amyloid-β deposition in the brain (Sperling *et al.*, 2011). Preclinical Alzheimer's disease is associated with future cognitive decline and mortality (Vos *et al.*, 2013); however, several neuropathological studies have shown no significant association between density of amyloid-β plaques and the severity of dementia or neuronal loss (Arriagada *et al.*, 1992; Bierer *et al.*, 1995; Gomez-Isla *et al.*, 1997), suggesting the involvement of other key factors in Alzheimer's disease-related neurodegeneration.

Neurofibrillary tangles are comprised of paired helical filaments that result from the abnormal aggregation of tau protein (Grundke-Iqbal *et al.*, 1986*a*, *b*; Lee *et al.*, 1991). Initial neurofibrillary tangle lesions occur in the trans-entorhinal cortex, followed by entorhinal cortex and hippocampus involvement, progressing to temporal neocortex and finally to the other neocortical areas (Arnold *et al.*, 1991; Braak and Braak, 1991). In contrast with senile plaques, neurofibrillary tangle formation correlates well with cognitive impairment severity (Arriagada *et al.*, 1992; Berg *et al.*, 1993; Bierer *et al.*, 1995), an association that is considered to continue throughout the disease course (Abner *et al.*, 2011). Furthermore, the inhibition of abnormal tau hyperphosphorylation and its aggregation appear to be promising therapeutic strategies in Alzheimer's disease. Thus, non-invasive imaging of tau pathology would be useful to assist in the early and differential diagnosis of dementia, track the progression of disease-related pathology, and monitor the efficacy of anti-tau treatments.

^{18}F-FDDNP has been reported to detect neurofibrillary tangle deposition (Shoghi-Jadid *et al.*, 2002) and successfully differentiate subjects with Alzheimer's disease and mild cognitive impairment from those with no cognitive impairment (Small *et al.*, 2006). However, this tracer detects the combined signals of senile plaques and neurofibrillary tangles (Shoghi-Jadid *et al.*, 2002). Several radiotracers have been developed for the selective visualization of neurofibrillary tangles in the living brain (Chien *et al.*, 2013, 2014; Maruyama *et al.*, 2013). Early clinical PET studies successfully differentiated patients with Alzheimer's disease from cognitively normal elderly. However, the selective binding ability of these radiotracers to tau has not been fully validated *in vivo*.

For the development of a selective tau radiotracer, we screened β-sheet-binding small molecules and identified novel quinoline derivatives with high binding selectivity to tau deposits in Alzheimer's disease brain samples (Okamura *et al.*, 2005; Fodero-Tavoletti *et al.*, 2011; Harada *et al.*, 2013). Through a compound optimization process, we developed a novel ^{18}F-labelled 2-arylquinoline derivative, ^{18}F-THK5105 (Fig. 1), which showed high binding affinity and selectivity to tau protein deposits in Alzheimer's disease brain sections (Okamura *et al.*, 2013). This ^{18}F-labelled radiotracer also exhibited high blood–brain barrier permeability and no defluorination in mice (Okamura *et al.*, 2013). The present clinical study evaluated whether ^{18}F-THK5105 PET could selectively bind to tau pathology in living patients with Alzheimer's disease.

Materials and methods

Participants

Sixteen subjects, including eight patients with probable Alzheimer's disease (three male and five females, age range 66–82 years) and eight age-matched healthy control subjects (three male and five females, age range 63–76 years), underwent both ^{18}F-THK5105 and ^{11}C-labelled Pittsburgh compound B (^{11}C-PiB) PET scans (Table 1). Written informed consent was obtained from all participants. Study approval was obtained from the Austin Health Human Research Ethics Committee. Elderly healthy controls were recruited by advertisements in the community, and patients with Alzheimer's disease were recruited from tertiary Memory Disorders Clinics or physicians who sub-specialize in dementia care. All participants were reviewed and classified on the basis of their clinical and neuropsychological performance by the consensus of a neurologist and a neuropsychologist who were blind to their PET results. The diagnosis of Alzheimer's disease was made according to the National Institute of Neurological and Communicative Disorders and Stroke/Alzheimer's Disease and Related Disorders Association (NINCDS-ADRDA) criteria.

Neuropsychological evaluation

Cognitive impairment and dementia severity were evaluated with the Mini-Mental State Examination (MMSE), the Clinical Dementia Rating (CDR) and the CDR scale sum of boxes (CDR-SOB). In addition, composite episodic memory and non-memory scores were generated as previously described (Villemagne *et al.*, 2011). Briefly, a composite episodic memory score was calculated by taking the average of the *z*-scores for the Rey Complex Figure Test, the long delay California Verbal Learning Test, Second Edition, and the Logical Memory II subscale of the Wechsler Memory Scale. A composite non-memory score was calculated by taking the average of the *z*-scores for the Boston Naming Test, letter fluency, category fluency, digit span forwards and backwards, digit symbol-coding, and Rey Complex Figure Test copy.

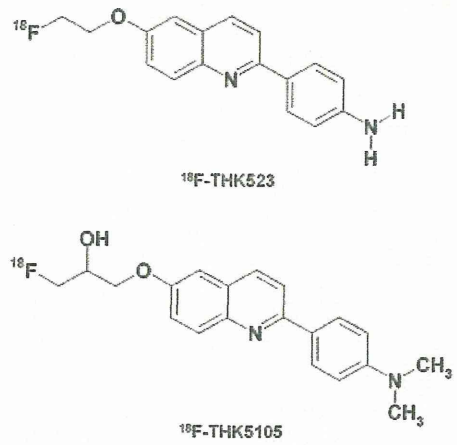

Figure 1 Chemical structures of ^{18}F-THK523 and ^{18}F-THK5105.

Table 1 Demographic characteristics of healthy control and Alzheimer's disease subjects

	Healthy controls ($n = 8$)	Alzheimer's disease ($n = 8$)
Age	70.5 ± 4.4	74.1 ± 6.9
Gender (M/F)	3/5	3/5
Years of education	15.4 ± 2.4	11.3 ± 3.2*
CDR	0.0	0.9 ± 0.5*
CDR-SOB	0.0	6.1 ± 4.9*
MMSE score	28.8 ± 1.5	17.3 ± 6.6*
Episodic memory scores	−0.1 ± 0.8	−3.8 ± 0.3*
Non-memory scores	−0.1 ± 0.5	−3.0 ± 1.9*
Grey matter volume (cm^3)	302.7 ± 12.9	272.9 ± 22.6*
Hippocampal volume (cm^3)	4.8 ± 0.5	4.0 ± 0.6*

*$P < 0.05$ by the Mann–Whitney U test.

Image acquisition

MRI scanning was performed on a 3 T Siemens TRIO magnetic resonance system (Siemens Healthcare) using the ADNI 3D MPRAGE sequence with 1 × 1 mm in-plane resolution and 1.2 mm slice thickness, repetition time/echo time/inversion time = 2300/2.98/900, flip angle 9°, field of view 240 × 256, and 160 slices. T_2 fast spin echo and FLAIR sequences were also obtained.

Two radiotracers, ^{18}F-THK5105 and ^{11}C-PiB, were prepared in the Centre for PET at Austin Hospital. ^{18}F-THK5105 was synthesized by nucleophilic substitution of the tosylate precursor as described previously (Okamura *et al.*, 2013). The decay-corrected average radiochemical yield of the production of ^{18}F-THK5105 was 45%, with a radiochemical purity >95% and a specific activity of 229.6 GBq/μmol (6.2 ± 3.3 Ci/μmol). ^{11}C-PiB was synthesized using the one-step ^{11}C-methyl triflate approach as previously described (Rowe *et al.*, 2007). The decay-corrected average radiochemical yield for ^{11}C-PiB was 30%, with a radiochemical purity >98% and a specific activity of 30 ± 7.5 GBq/μmol.

A list-mode emission acquisition on an Allegro™ PET camera (Philips Medical Systems) was performed in 3D mode from 0–50 min and between 90–120 min after injection of 200 MBq ^{18}F-THK5105. List-mode raw data for the initial 50 min of the acquisition were sorted off-line into 6 × 30-s, 7 × 1-min, 4 × 2.5-min, 2 × 5-min, and 6 × 10-min frames. The final 30 min were acquired as 6 × 5-min frames. The sorted sinograms were reconstructed using a 3D RAMLA algorithm. A 30-min acquisition (6 × 5-min frames) on an Allegro™ PET camera began 40 min after intravenous injection of 300 MBq ^{11}C-PiB.

Image analysis

Hippocampal and cortical grey matter volumes were obtained using an automated volumetric measurement program (NeuroQuant: CorTechs Labs Inc) applied to the 3D MP RAGE MRI images. The primary MRI outcome measures were the grey cortical matter and hippocampal volumes normalized to total intracranial volume.

PET images were processed using a semi-automatic region of interest method. Firstly, standardized uptake value (SUV) images of ^{18}F-THK5105 and ^{11}C-PiB were obtained by normalizing tissue radioactivity concentration by injected dose and body weight. Subsequently, individual MRI T_1 images were anatomically co-registered into individual PET images using Statistical Parametric Mapping software (SPM8: Wellcome Trust Centre for Neuroimaging, London, UK). Co-registered MRI and PET images were then spatially normalized to an MRI T_1 template in Talairach space using SPM8. After spatial normalization, a region of interest template was placed on individual axial images in the cerebellar hemisphere, ventrolateral frontal cortex [Brodmann areas (BA) 10, 44, 45 and 46], lateral and medial orbitofrontal cortex (BA 11 and 12), superior temporal cortex (BA 22), inferior temporal cortex (BA 20 and 37), parietal cortex (BA 39 and 40), lateral occipital cortex (BA 18 and 19), anterior cingulate cortex, posterior cingulate cortex, mesial temporal cortex (BA 27, 28, 34 and 35), putamen, pons, and subcortical white matter. Regional SUVs were sampled using PMOD software (PMOD Technologies, Ltd).The ratio of regional SUV to cerebellar cortex SUV ratio (SUVR) was used as an index of tracer retention. Neocortical tau and amyloid-β burden were expressed as the average SUVR for the following cortical regions of interest: frontal, parietal, lateral temporal, and posterior cingulate for THK5105 and PiB, respectively. As in previous studies, a PiB SUVR threshold of 1.5 was used to categorize high and low amyloid-β burden.

Statistical analysis

Mann-Whitney's U-tests were applied for comparison of the Alzheimer's disease and healthy control groups. For comparison of regional radiotracer uptake, one-way repeated measures analysis of variance (ANOVA) followed by Bonferroni's tests were performed. To examine the regional difference of tracer retention between neocortex and mesial temporal cortex, Wilcoxon matched-pairs signed rank tests were performed. Effect size coefficients (Cohen's d) were calculated for the evaluation of group differences in PET measurements. Statistical significance for each analysis was defined as $P < 0.05$. Data are presented as mean ± standard deviation (SD).

Results

Healthy control and Alzheimer's disease subject demographics are shown in Table 1. There were no significant differences between healthy control and Alzheimer's disease groups with regard to age

or gender; however, the Alzheimer's disease group was significantly less educated than the healthy control group. As expected, significant differences between the two groups were observed for CDR and CDR-SOB scores, cognitive performance (MMSE, episodic memory, and non-memory scores), and brain volumetrics (grey matter and hippocampal volumes).

No toxic event was observed in the current clinical PET study. After intravenous administration of ^{18}F-THK5105, all subjects showed rapid entry of the tracer into grey matter areas. The SUV time activity curves of ^{18}F-THK5105 PET are shown in Fig. 2. The peak uptake and clearance rates of ^{18}F-THK5105 in the cerebellar cortex were similar between healthy control (Fig. 2A) and Alzheimer's disease (Fig. 2B) groups. In patients with Alzheimer's disease, the inferior temporal cortex, which is an area known to contain high densities of neurofibrillary tangles in Alzheimer's disease (Bouras *et al.*, 1994), showed ^{18}F-THK5105 retention compared to the cerebellum, especially at the later time points. In contrast, time activity curves in the inferior temporal cortex of healthy control subjects were nearly identical to those in the cerebellum. The subcortical white matter region showed relatively lower entry and slower clearance than grey matter areas, but no significant differences were observed for time activity curves between healthy control and Alzheimer's disease groups (data not shown). The ratio of inferior temporal cortex to cerebellar SUVR became constant in all participants ~90 min after injection of ^{18}F-THK5105 (Fig. 2C). Therefore, we selected SUVR values from 90–100 min post-injection for the following analysis.

Summed SUVR images from 90–100 min post-injection for healthy control and Alzheimer's disease subjects are shown in Fig. 3. Contrasted with a lack of remarkable ^{18}F-THK5105 retention in the grey matter of healthy control subjects, patients with Alzheimer's disease showed high grey matter ^{18}F-THK5105 retention in the lateral and mesial temporal regions. ^{18}F-THK5105 retention was additionally observed in the brain stem; however, similar retention in these areas was detected in healthy control subjects. When comparing the 90–100 min regional SUVR in Alzheimer's disease and healthy control subjects, ^{18}F-THK5105 SUVRs for the ventrolateral prefrontal, medial orbitofrontal, superior, and inferior temporal, parietal, posterior cingulate, and mesial temporal cortices were significantly higher in patients with Alzheimer's disease (Table 2 and Fig. 4). Notably, SUVR in the inferior temporal cortex showed no overlap between the Alzheimer's disease and healthy control groups (Fig. 4). ^{18}F-THK5105 retention in other neocortical areas was relatively lower than in the inferior temporal area. The SUVR in the parietal cortex was elevated in 62.5% (5/8) of patients with Alzheimer's disease; however, ^{18}F-THK5105 retention in the ventrolateral prefrontal cortex was only elevated in 37.5% (3/8) of patients with Alzheimer's disease. Mesial temporal ^{18}F-THK5105 retention was significantly higher in patients with Alzheimer's disease than in healthy control subjects. However, a substantial overlap of SUVR was observed between both groups. The SUVR values in the pons and subcortical white matter were nearly identical in both groups, but higher than other neocortical regions. The effect size value between Alzheimer's disease and healthy control subjects was highest in the inferior temporal cortex, followed by the superior temporal, posterior cingulate, parietal, and medial orbitofrontal cortices and was lowest in the other regions examined (Table 2). Regional difference of ^{18}F-THK5105 retention was additionally examined in healthy control subjects. As a result, mesial temporal ^{18}F-THK5105 retention (mean SUVR = 1.17) was significantly higher than neocortical ^{18}F-THK5105 retention (mean SUVR = 1.05) in healthy control subjects.

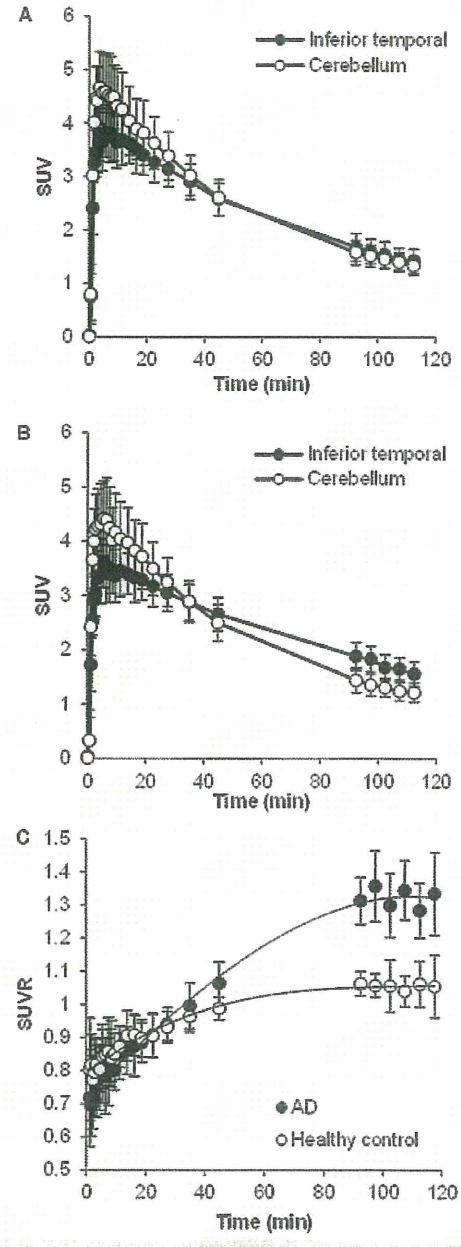

Figure 2 (**A** and **B**) ^{18}F-THK5105 SUV TACs in the cerebellum (open circles) and inferior temporal cortex (filled circles) of eight healthy control subjects (**A**) and eight patients with Alzheimer's disease (**B**). (**C**) SUVR time activity curves of ^{18}F-THK5105 PET in eight healthy control subjects (open circles) and eight patients with Alzheimer's disease (AD) (filled circles). Each point represents the mean ± SD.

As reported in previous PET studies (Klunk *et al.*, 2004; Mintun *et al.*, 2006; Rowe *et al.*, 2007), ^{11}C-PiB SUVR values were significantly greater in the neocortical regions of patients with Alzheimer's disease compared to healthy control subjects (Table 3). All patients with Alzheimer's disease showed marked and extensive PiB retention in neocortical areas. On the other hand, neocortical PiB retention in healthy control subjects was not significant, except for one healthy control case that only showed high ^{11}C-PiB retention in the frontal cortex. In contrast

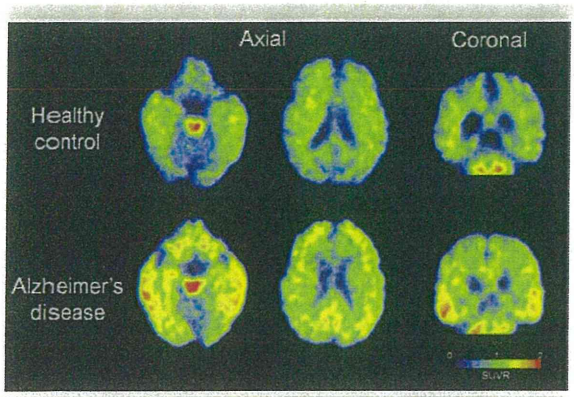

Figure 3 ^{18}F-THK5105 PET images from 60–80 min post-injection in a healthy control subject (72-years-old, CDR 0, MMSE 29) and a patient with Alzheimer's disease (68-years-old, CDR 1.0, MMSE 20).

Table 2 Regional ^{18}F-THK5105 SUVR values in healthy control and Alzheimer's disease subjects

Region	Healthy controls	Alzheimer's disease	Cohen's d
Ventrolateral prefrontal	1.08 ± 0.08	1.23 ± 0.14*	1.33
Lateral orbitofrontal	1.01 ± 0.08	1.15 ± 0.13	1.32
Medial orbitofrontal	1.17 ± 0.06	1.29 ± 0.09*	1.55
Superior temporal	1.04 ± 0.06	1.22 ± 0.07*	2.75
Inferior temporal	1.09 ± 0.04	1.32 ± 0.08*	3.58
Parietal	0.99 ± 0.08	1.16 ± 0.13*	1.59
Lateral occipital	1.07 ± 0.06	1.18 ± 0.15	1.01
Anterior cingulate	1.07 ± 0.11	1.12 ± 0.13	0.35
Posterior cingulate	1.04 ± 0.08	1.20 ± 0.12*	1.61
Mesial temporal	1.17 ± 0.05	1.26 ± 0.10*	1.17
Putamen	1.41 ± 0.10	1.52 ± 0.17	0.83
Pons	1.88 ± 0.14	1.89 ± 0.23	0.03
Subcortical white matter	1.22 ± 0.15	1.22 ± 0.15	0.01
Neocortex	1.05 ± 0.05	1.23 ± 0.08*	2.68

*$P < 0.05$ by the Mann–Whitney U test.

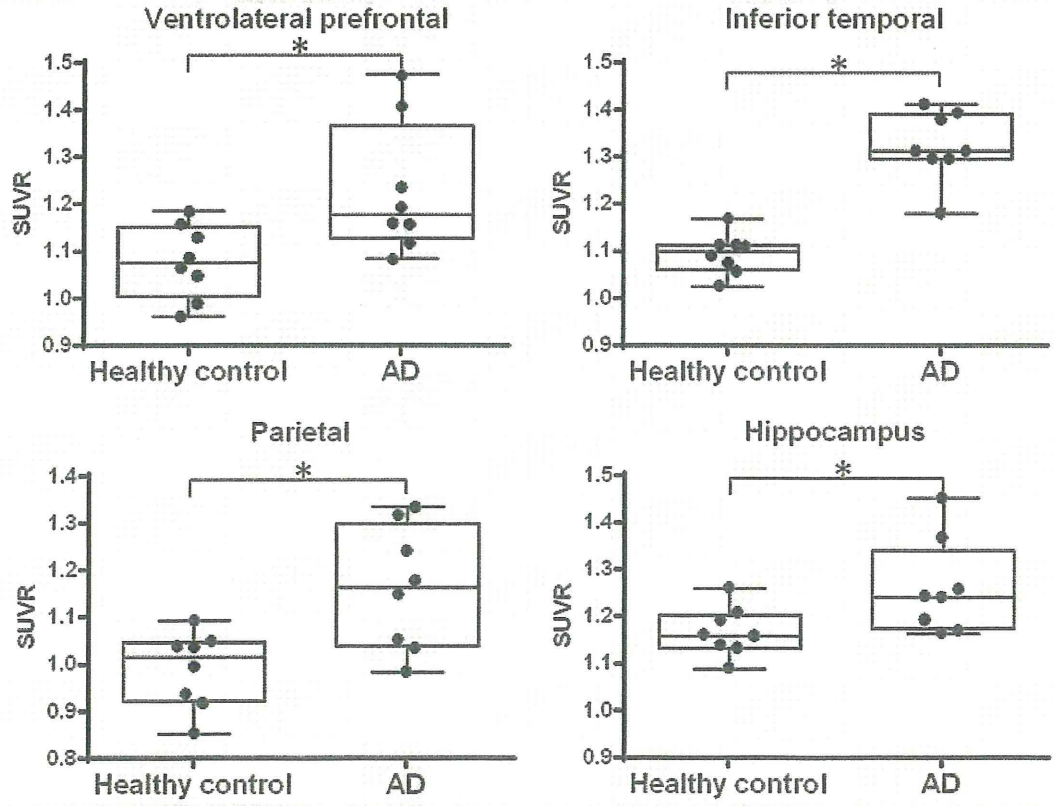

Figure 4 Regional ^{18}F-THK5105 SUVR values from 60–80 min post-injection in healthy control and Alzheimer's disease (AD) subjects. *$P < 0.05$ by the Mann–Whitney U test.

Table 3 Regional ^{11}C-PiB SUVR values in healthy control and Alzheimer's disease subjects

Region	Healthy controls	Alzheimer's disease	Cohen's d
Ventrolateral prefrontal	1.32 ± 0.39	2.92 ± 0.82*	2.49
Lateral orbitofrontal	1.08 ± 0.25	1.66 ± 0.50*	1.46
Medial orbitofrontal	1.36 ± 0.23	2.38 ± 0.63*	2.15
Superior temporal	1.11 ± 0.13	2.67 ± 0.67*	3.22
Inferior temporal	1.08 ± 0.08	2.42 ± 0.66*	2.88
Parietal	1.22 ± 0.17	2.56 ± 0.51*	3.54
Lateral occipital	1.25 ± 0.11	2.07 ± 0.61*	1.86
Anterior cingulate	1.39 ± 0.28	2.79 ± 0.70*	2.64
Posterior cingulate	1.31 ± 0.24	3.15 ± 0.78*	3.22
Mesial temporal	1.29 ± 0.15	1.65 ± 0.32*	1.42
Putamen	1.48 ± 0.20	2.64 ± 0.62*	2.50
Pons	2.04 ± 0.33	2.04 ± 0.40	0.00
Subcortical white matter	2.02 ± 0.38	2.06 ± 0.66	0.07
Neocortex	1.21 ± 0.14	2.75 ± 0.66*	3.21

*$P < 0.05$ by the Mann–Whitney U test.

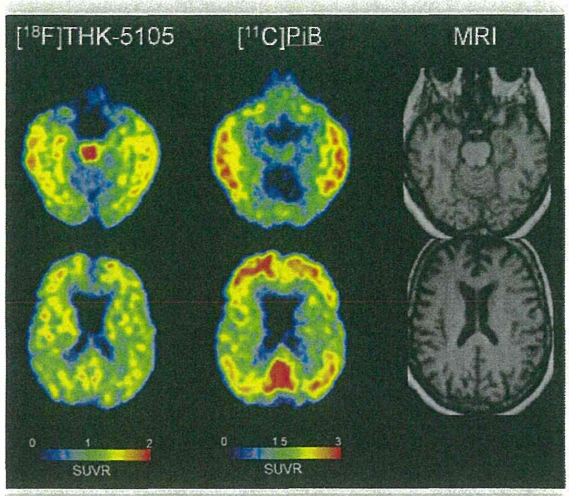

Figure 5 ^{18}F-THK5105 PET images from 60–80 min post-injection and ^{11}C-PiB PET images from 40–70 min post-injection in an Alzheimer's disease patient (68-years-old, CDR 1.0, MMSE 20). Co-registered magnetic resonance images are shown on the right.

with the highest neocortical ^{18}F-THK5105 retention in the inferior temporal cortex of patients with Alzheimer's disease, ^{11}C-PiB retention in the same group was highest in the posterior cingulate cortex, followed by the ventrolateral prefrontal, anterior cingulate, and superior temporal cortices. The PiB effect size value between Alzheimer's disease and healthy control subjects was also highest in the parietal cortex, followed by the posterior cingulate and superior temporal cortices. As shown in Fig. 5, the pattern of cortical ^{18}F-THK5105 retention was completely different from that of ^{11}C-PiB retention in patients with Alzheimer's disease, which was prominent in the frontal cortex and precuneus, but not evident in the mesial temporal cortex. In contrast, ^{18}F-THK5105 retention was evident in both lateral and mesial temporal areas but not so remarkable in other neocortical areas. There was no correlation between neocortical ^{18}F-THK5105 and ^{11}C-PiB SUVR values in patients with Alzheimer's disease ($r = 0.17$, $P = 0.703$). In addition, one healthy control case showing elevated PiB retention in the frontal cortex did not show any significant retention of ^{18}F-THK5105.

Finally, we explored the relationship of neocortical or mesial temporal radiotracer retention to cognitive parameters in patients with Alzheimer's disease. Neocortical ^{18}F-THK5105 retention was significantly correlated with MMSE scores ($r = -0.781$, $P = 0.022$), CDR ($r = 0.730$, $P = 0.050$) and CDR-SOB ($r = 0.779$, $P = 0.030$), but not correlated with composite episodic memory and non-memory scores. In contrast, neocortical ^{11}C-PiB retention showed no significant correlation with any cognitive parameters (Fig. 6). There was no correlation between radiotracer retention in mesial temporal cortex and cognitive parameters. Furthermore, we explored the relationship of radiotracer retention with brain volumetrics. When all subjects were included in the analysis, a significant correlation was observed between mesial temporal ^{18}F-THK5105 retention and hippocampal volumes ($r = -0.565$, $P = 0.023$) and between neocortical ^{18}F-THK5105 retention and whole brain grey matter volumes ($r = -0.649$, $P = 0.007$). When only patients with Alzheimer's disease were included in this analysis, hippocampal volumes were significantly correlated with neocortical ^{18}F-THK5105 retention ($r = -0.765$, $P = 0.027$), but not correlated with mesial temporal ^{18}F-THK5105 retention. However, there were no correlations between mesial temporal ^{11}C-PiB retention and hippocampal volumes and between neocortical ^{11}C-PiB retention and whole brain grey matter volumes (Fig. 7).

Discussion

In this study, the novel radiotracer ^{18}F-THK5105 successfully differentiated patients with Alzheimer's disease from healthy control subjects. The pattern of ^{18}F-THK5105 distribution in patients with Alzheimer's disease appears similar to the reported neurofibrillary tangle distribution in the post-mortem Alzheimer's disease brain. ^{18}F-THK5105 retention in the inferior temporal cortex, where neurofibrillary tangle accumulation is highest in Alzheimer's disease, was observed in most patients with Alzheimer's disease. In contrast to the high frequency of ^{18}F-THK5105 retention in the temporal cortices of Alzheimer's disease cases, ventrolateral prefrontal ^{18}F-THK5105 retention was less frequent (3/8) and was only observed in cases with moderate-to-severe Alzheimer's disease (MMSE range 10–17). This finding is consistent with neurofibrillary tangle distribution in post-mortem Alzheimer's disease brain, where there is a higher frequency of neurofibrillary tangles in the temporal cortex than the frontal cortex (Arnold *et al.*, 1991; Bouras *et al.*, 1994; Haroutunian *et al.*, 1999). It is also in agreement with recent PET results using other novel radiotracers (^{18}F-T807 and ^{18}F-T808) that demonstrated higher radiotracer retention in the lateral temporal lobe compared to the frontal lobe and selective binding ability to paired helical filament tau (Chien *et al.*, 2013, 2014). These findings suggest a spreading